ISSN 1560-3547, Regular and Chaotic Dynamics, 2016, Vol. 21, Nos. 7–8, pp. 885–901. © Pleiades Publishing, Ltd., 2016.

Regular and Chaotic Dynamics in the Rubber Model of a Chaplygin Top

Alexey V. Borisov[1*], Alexey O. Kazakov[2], and Elena N. Pivovarova[1***]**

[1] *Udmurt State University,*
ul. Universitetskaya 1, Izhevsk, 426034 Russia

[2] *National Research University Higher School of Economics,*
ul. Bolshaya Pecherskaya 25/12, Nizhny Novgorod, 603155 Russia

Received November 21, 2016; accepted December 06, 2016

Abstract—This paper is concerned with the rolling motion of a dynamically asymmetric unbalanced ball (Chaplygin top) in a gravitational field on a plane under the assumption that there is no slipping and spinning at the point of contact. We give a description of strange attractors existing in the system and discuss in detail the scenario of how one of them arises via a sequence of period-doubling bifurcations. In addition, we analyze the dynamics of the system in absolute space and show that in the presence of strange attractors in the system the behavior of the point of contact considerably depends on the characteristics of the attractor and can be both chaotic and nearly quasi-periodic.

MSC2010 numbers: 37J60, 37G35, 70E18

DOI: 10.1134/S156035471607011X

Keywords: Chaplygin top, nonholonomic constraint, rubber model, strange attractor, bifurcation, trajectory of the point of contact

INTRODUCTION

1. The study of the rolling motion of a dynamically asymmetric balanced ball on a plane was started by S. A. Chaplygin in [23] and continued in [12, 16, 36]. Due to the integrability of this problem the dynamical characteristics of the system exhibit regular behavior and can be analyzed using well-developed qualitative and topological methods. One of the possible generalizations of this system is the problem of a Chaplygin ball rolling on a sphere; this problem is much more complicated, and is investigated in [6, 18].

The surface for which the classical no-slip constraint is realized at the point of contact is called, according to the terminology of J. Koiller and K. Ehlers [26], the "marble" (marble rolling) model. For ease of analysis of rolling motion, a different surface model is used in various areas, in particular, in robotics, which, according to the same terminology, is called the "rubber" (rubber rolling) model and which imposes, along with the no-slip constraint, a no-spin constraint, i. e., the projection of the angular velocity onto the normal to the surface is zero. A detailed treatment of this model can be found in [20]. The rubber and marble models have both similarities and differences. The hierarchy of behaviors of dynamical systems in the marble model is examined in detail in [19, 22]. We note that the rubber model, although it is simpler than the marble model, has been very poorly studied. Both the marble and the rubber model of rolling assume the presence of nonintegrable constraints and can be examined by modern methods of nonholonomic mechanics. For the historical development and the basic facts of this science we refer the reader to the recent review [21].

The problem of the motion of a dynamically asymmetric ball with a displaced center of mass in a gravitational field using the rubber model has not been systematically studied before (moreover,

*E-mail: borisov@rcd.ru
**E-mail: kazakovdz@ya.ru
***E-mail: archive@rcd.ru

even a balanced ball was not considered, although this problem is integrable by quadratures). Some explanations of the rubber model for the rolling motion of a Chaplygin ball have been given recently in [31], however, this problem requires further study. In this paper, we shall call the model of a Chaplygin ball with a displaced center of mass the *Chaplygin top*. We note that for the marble model of the Chaplygin top the authors of [8, 40] point out the existence of figure-eight and spiral strange attractors, as well as a strange attractor arising due to destruction of the quasi-periodic regime. The rubber model of such a system is only beginning to be explored [34, 35]. For example, in [34] an attractor of unusual form was found, which is in fact a quasi-attractor [1], moreover, local and global bifurcations giving rise to this attractor were investigated. In [35], the influence of constant gyrostatic momentum on the chaotic dynamics of the system was explored.

2. In this paper, we take a more systematic approach to the investigation of the dynamics of the Chaplygin top by analyzing the chart of dynamical regimes of the system, which allows one not only to find strange attractors, but also to keep track of the scenarios of their birth. The analysis carried out by us has allowed us to find a strange Feigenbaum attractor; the transition to this attractor occurs via a sequence of period-doubling bifurcations. We note that the system of interest exhibits weak dissipation and large multistability (when a variety of different attractors coexist in the phase space of the system). As a consequence, the construction of regime charts and the calculation of universal constants lead to laborious calculations. We note that specific dissipation (arising due to nonholonomic constraints) is, as a rule, due to the presence of various involutions and can lead to strange attractors. However, it is quite probable that not all attractors that may arise from general theory are realized in nonholonomic systems. Since their presence has a considerable influence on the dynamics (for example, on the trajectory of the point of contact), the problem of finding and exploring them is important and requires a separate study.

3. One of the important avenues of research is the study of the behavior of the contact point, since the trajectory of the ball is important for analysis of the system dynamics and can be used for comparison with experimental data. For the balanced Chaplygin ball in the rubber model, due to additional restrictions (imposed on the position of the center of mass), all trajectories of motion have a directed drift with transverse oscillations (see Fig. 1a). In the case of a displaced center of mass, but with zero gravitational field, the system possesses an additional integral [17], but in this case there is no smooth invariant measure [3, 4]. The topological integral foliation is isomorphic to the Euler – Poinsot case in rigid body dynamics, but the distribution of rotation numbers forms a Cantor ladder, which is an obstruction to integrability by quadratures. The behavior of the contact point in this case is regular and bounded (see Fig. 1b).

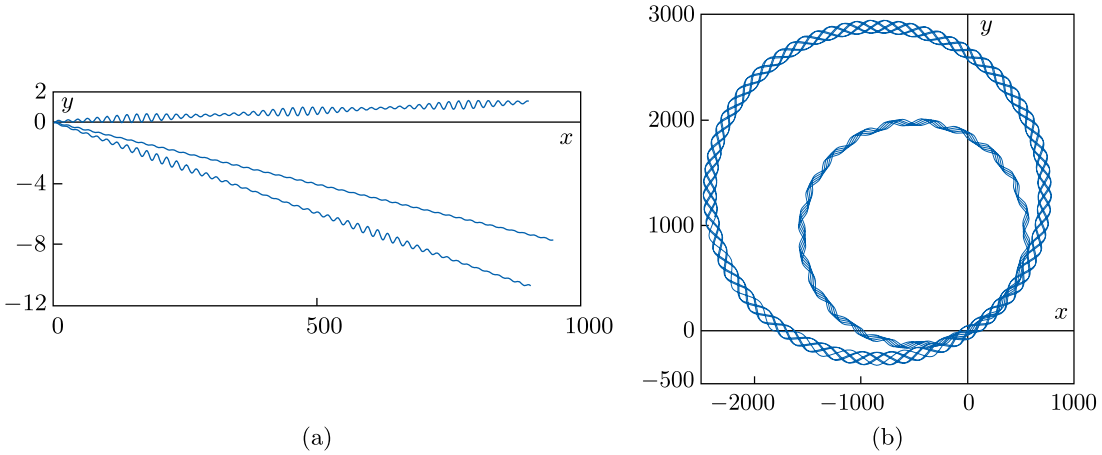

Fig. 1. Typical trajectories of a balanced dynamically asymmetric ball moving on a plane in a gravitational field (a) and those of an unbalanced dynamically asymmetric ball with zero gravitational field (b).

In the problem under consideration, although several attractors, including complex ones, exist in the phase space of the reduced system, the behavior of the contact point can be close to quasi-periodic motion near which chaotic oscillations with an extremely small amplitude occur. In this

paper, we show that the behavior of the contact point for the Chaplygin top depends not only on the nature of the attractor (chaoticity or regularity), but also on its characteristics, such as dimension indices of the attractor, Lyapunov exponents etc. For the chaotic behavior of the contact point we calculate various parameters which characterize the diffusion (random pattern of trajectories) and directed motion. The almost regular behavior of the contact point even in the case of classical attractors shows that the appearance of strange attractors in approximate Lorenz type models does not necessarily lead to observation of real chaotic behavior of the system.

We note that the problem considered in this paper has a model character. Its investigation is important both for dynamical systems theory (for understanding the birth and the role of attractors in dynamical systems) and for robotics and control theory, since the problem of controlling spherical bodies (spherical robots) has given rise to a large amount of research recently (see, for example, [2, 10, 11, 24, 25] and references therein). We also note that the irregularity of the behavior of the contact point can be used to create a directed drift. Therefore, the problem of drift and diffusion of the contact point in the modern concept can be used to control chaos [38], although it should be noted that so far this idea has hardly taken hold in mechanical systems (except perhaps for celestial mechanics [37]). More advanced studies have been carried out only for the control of regular systems [10, 11].

1. EQUATIONS OF MOTION AND FIRST INTEGRALS

Consider the motion of a dynamically asymmetric unbalanced ball (Chaplygin top) on a horizontal plane (Fig. 2). To describe the dynamics of the system, we choose a fixed coordinate system $O\boldsymbol{\alpha}\boldsymbol{\beta}\boldsymbol{\gamma}$ and a moving coordinate system $C\boldsymbol{\xi}\boldsymbol{\eta}\boldsymbol{\zeta}$ attached to the body with axes directed along the principal axes of inertia. The connection between the fixed and moving coordinate systems is given by the transfer matrix $\mathbf{Q} = (\boldsymbol{\alpha}, \boldsymbol{\beta}, \boldsymbol{\gamma})$. Let o denote the geometric center of the ball, C its center of mass, and $\boldsymbol{a} = (a_1, a_2, a_3)$ the vector of displacement of the ball's center of mass relative to the geometric center. Here and below, unless otherwise specified, all vectors (highlighted in bold face) are referred to the moving coordinate system $C\boldsymbol{\xi}\boldsymbol{\eta}\boldsymbol{\zeta}$.

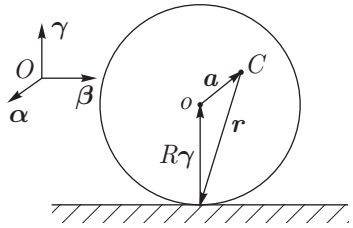

Fig. 2

We shall specify the position of the system by the coordinates of the center of mass of the ball $\boldsymbol{r}$ and its orientation in space by the matrix $\mathbf{Q}$. Thus, the configuration space of the system is the product $\mathcal{N} = \{\boldsymbol{r}, \mathbf{Q}\} = \mathbb{R}^3 \times SO(3)$.

We shall assume that no-slip and no-spin constraints have been imposed on the system at the point of contact of the ball with the surface. These constraints are described by the equations

$$\boldsymbol{v} + \boldsymbol{\omega} \times \boldsymbol{r} = 0, \qquad (\boldsymbol{\omega}, \boldsymbol{\gamma}) = 0,$$

where $\boldsymbol{r}$ is the radius vector connecting the center of mass with the contact point, $\boldsymbol{v}$, $\boldsymbol{\omega}$ is the velocity of the center of mass and the angular velocity of the ball, and $\boldsymbol{\gamma}$ is the normal vector to the surface at the contact point.

The equations of motion which govern the evolution of the variables $\boldsymbol{\omega}$ and $\boldsymbol{\gamma}$ have the form [17]

$$\widetilde{\mathbf{I}}\dot{\boldsymbol{\omega}} = \widetilde{\mathbf{I}}\boldsymbol{\omega} \times \boldsymbol{\omega} - m\boldsymbol{r} \times (\boldsymbol{\omega} \times \dot{\boldsymbol{r}}) + mg(\boldsymbol{\gamma} \times \boldsymbol{a}) + \lambda_0\boldsymbol{\gamma}, \qquad \dot{\boldsymbol{\gamma}} = \boldsymbol{\gamma} \times \boldsymbol{\omega},$$
$$\lambda_0 = -\frac{\left(\widetilde{\mathbf{I}}^{-1}\boldsymbol{\gamma}, \widetilde{\mathbf{I}}\boldsymbol{\omega} \times \boldsymbol{\omega} - m\boldsymbol{r} \times (\boldsymbol{\omega} \times \dot{\boldsymbol{r}}) + mg(\boldsymbol{\gamma} \times \boldsymbol{a})\right)}{(\boldsymbol{\gamma}, \widetilde{\mathbf{I}}^{-1}\boldsymbol{\gamma})}, \tag{1.1}$$

where $\widetilde{\mathbf{I}} = \mathbf{I} + m(\boldsymbol{r},\boldsymbol{r})\cdot\mathbf{E} - m\boldsymbol{r}\cdot\boldsymbol{r}^T$ is the tensor of inertia of the ball relative to the point of contact, $\mathbf{I} = \operatorname{diag}(I_1, I_2, I_3)$ is the tensor of inertia of the ball, written in terms of the coordinate system attached to the ball, m is the mass of the ball, and g is the free-fall acceleration.

Supplementing Eqs. (1.1) with kinematic relations describing the trajectory of the contact point of the ball and its orientation

$$\begin{aligned} \dot{x} &= R(\boldsymbol{\beta},\boldsymbol{\omega}), \qquad \dot{y} = -R(\boldsymbol{\alpha},\boldsymbol{\omega}),\\ \dot{\boldsymbol{\alpha}} &= \boldsymbol{\alpha}\times\boldsymbol{\omega}, \qquad \dot{\boldsymbol{\beta}} = \boldsymbol{\beta}\times\boldsymbol{\omega}, \end{aligned} \tag{1.2}$$

we obtain a closed system of equations which completely describes the motion of the ball on the plane.

The radius vector of the center of mass $\boldsymbol{r}$ can be expressed in terms of the normal vector to the surface at the point of contact in the form

$$\boldsymbol{r} = -R\boldsymbol{\gamma} - \boldsymbol{a}.$$

In view of this relation, we note that Eqs. (1.1) depend only on the variables $\boldsymbol{\omega}$ and $\boldsymbol{\gamma}$ and hence form a closed reduced system of equations.

The system of Eqs. (1.1) possesses two first integrals:

the energy integral $$\mathcal{E} = \frac{1}{2}(\boldsymbol{\omega}, \widetilde{\mathbf{I}}\boldsymbol{\omega}) - mg(\boldsymbol{r},\boldsymbol{\gamma}),$$

the geometric integral $$(\boldsymbol{\gamma},\boldsymbol{\gamma}) = 1,$$

moreover, in this system the no-spin constraint can also be regarded as a particular integral:

$$(\boldsymbol{\omega},\boldsymbol{\gamma}) = 0.$$

The most convenient variables for numerical investigation of the dynamics of the system of interest are the Andoyer – Deprit variables [14, 15], which are related to $\boldsymbol{\omega}$ and $\boldsymbol{\gamma}$ by

$$\begin{aligned} \omega_1 &= \sqrt{G^2 - L^2}\sin l,\\ \omega_2 &= \sqrt{G^2 - L^2}\cos l,\\ \omega_3 &= L,\\ \gamma_1 &= \frac{L}{G}\cos g\sin l + \sin g\cos l,\\ \gamma_2 &= \frac{L}{G}\cos g\cos l - \sin g\sin l,\\ \gamma_3 &= -\sqrt{1 - \left(\frac{L}{G}\right)^2}\cos g. \end{aligned}$$

The introduction of these variables decreases the dimension of the system to four, since the existence of a geometric integral and an integral realizing the no-spin constraint was taken into consideration from the outset. Thus, on the level set of the energy integral, the dynamics of the system is described in the Andoyer – Deprit variables using a three-dimensional flow whose section in the variable $g = \text{const}$ gives a two-dimensional Poincaré map on the plane $(l, L/G)$.

2. DESCRIPTION OF ATTRACTORS EXISTING IN THE SYSTEM

As shown in the paper [34] of one of the authors, for the following parameters

$$\begin{gathered} E = 50, \quad R = 3, \quad m = 1, \quad \mathrm{g} = 9.77145\\ I_1 = 1, \quad I_2 = 2, \quad I_3 = 3,\\ a_1 = 1, \quad a_2 = 1.5, \quad a_3 = 0.5 \end{gathered}$$

the system has a strange chaotic attractor (quasi-attractor [1]), which is shown in Fig. 3a (we shall call it *attractor I*). In the course of further numerical investigation of the Poincaré map, under a

small change in the displacement of the center of mass a_3, an attractor was found whose portrait is shown in Fig. 3b (*attractor II*). This attractor exists for the following system parameters:

$$E = 50, \quad R = 3, \quad m = 1, \quad \mathrm{g} = 9.77145$$
$$I_1 = 1, \quad I_2 = 2, \quad I_3 = 3,$$
$$a_1 = 1, \quad a_2 = 1.5, \quad a_3 = 0.9.$$

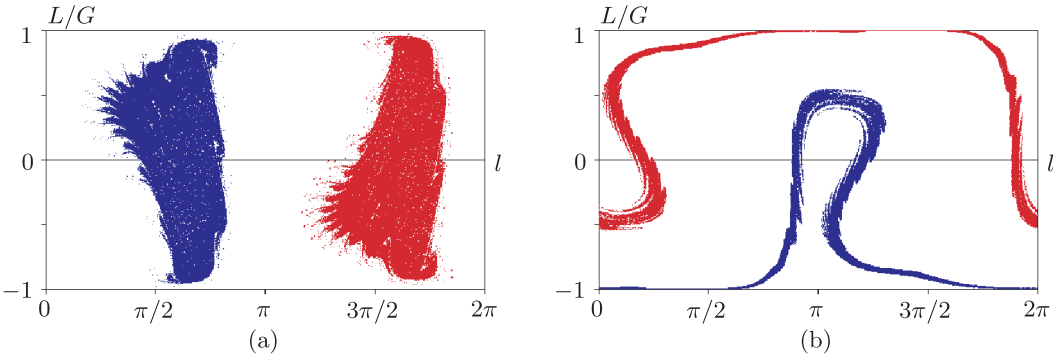

Fig. 3. Portraits of attractors in the Poincaré section for a Chaplygin top, which have been obtained for the parameter $E = 50$, $R = 3$, $m = 1$, $\mathrm{g} = 9.77145$, $I_1 = 1$, $I_2 = 2$, $I_3 = 3$, $a_1 = 1$, $a_2 = 1.5$, and (a) $a_3 = 0.5$, (b) $a_3 = 0.9$. Blue denotes an attractor, red corresponds to a repeller constructed in backward time.

Bifurcations giving rise to attractor I are described in detail in [34]. We note that this attractor arises not according to one of the well-known scenarios, but via a complex sequence of global and local bifurcations. In what follows we consider in detail the scenario of birth of attractor II and explore the dynamics of the system in absolute space with parameters corresponding to the existence of this attractor.

3. SCENARIO OF BIRTH OF A NEW ATTRACTOR

In this section, we shall describe the scenario of birth of a chaotic attractor shown in Fig. 3b. We shall keep track of changes in the dynamical behavior of the system by varying the parameters a_3 and g with constant values of the other parameters and by analyzing the charts of dynamical regimes and Lyapunov exponents [7].

The chart of regimes is the diagram on a parameter plane (in our case (a_3, g)) each point of which is colored in a certain way. It is constructed using the following algorithm (which is analogous, for example, to that presented in [7]). A pair of parameters is assigned to each node of the chart. For given parameters one calculates some number of iterations of the Poincaré map (in our case case $2 \cdot 10^4$), then the resulting point is checked for periodicity and this procedure is repeated for the subsequent parameter values. The final state of the system obtained in the previous step is used as initial conditions (inheritance of initial conditions). If the period of the point is defined in the interval from 1 to 160, the corresponding node of the chart is colored in a certain way according to the scale located near the chart. If the point has a higher period or its trajectory is not periodic, the corresponding node is colored grey. The chart of Lyapunov exponents is a diagram that is quite similar to the chart of dynamical regimes. The difference is that for each pair of parameters of the chart of Lyapunov exponents we calculate the largest Lyapunov exponent (LLE). If the value of LLE is positive, we indicate the corresponding node on the chart by a shade of red, and if LLE is negative, we indicate the node by a shade of blue.

A preliminary analysis has revealed a point of period 19, which is born as a result of a saddle-node bifurcation. This point exists in a relatively wide range of parameters a_3 and g and, as we will show below, a Feigenbaum attractor is born from it via a sequence of period-doubling bifurcations. Therefore, in this paper we will consider a neighborhood of the parameters at which this point was detected.

Figure 4 shows a chart of dynamical regimes of the Poincaré map and a chart of Lyapunov exponents for the Chaplygin top. This chart has been constructed on the parameter plane (a_3, g).

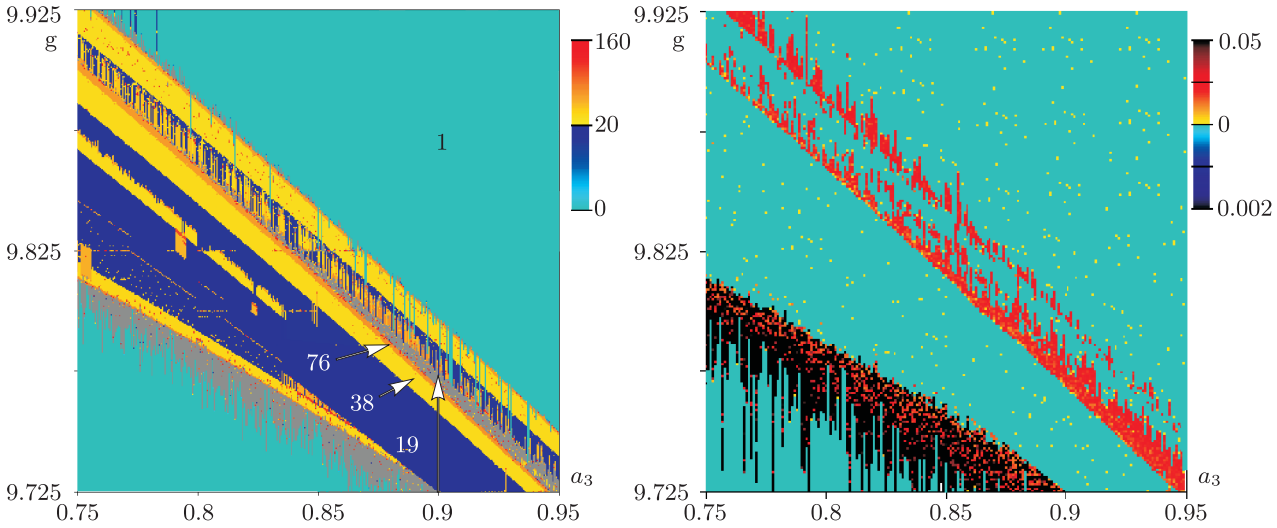

Fig. 4. (a) Chart of regimes on the parameter plane (a_3, g). The numbers on the chart denote periods of stable points. Red denotes points corresponding to stable motions of period 152. (b) Chart of Lyapunov exponents.

The above-mentioned point of period 19 exists in a fairly wide region of the chart, which is colored dark blue.

In [34] it was shown that the dynamics of the Chaplygin top exhibits developed multistability, that is, at the same parameters there coexist many periodic regimes in the system; these regimes appear and disappear as a result of saddle-node bifurcations under small changes in the parameters. As a consequence, the chart shown in Fig. 4 consists of several pieces each of which has been constructed so that the initial conditions are inherited from the point of period 19.

If one moves on the chart by changing the parameters from below upwards and from left to right from the region corresponding to the fixed point of period 19, one can observe a sequence of period-doubling bifurcations of the fixed points 19–38–76–152 and a transition to chaos according to the Feigenbaum scenario [27]. Next, we present the portraits of attractors for each of the regimes at the constant value $a_3 = 0.9$ and under changes of the parameter g (i.e., we shall move from below upwards on the chart along the vertical arrow).

Figure 5 shows the phase portraits on the Poincaré map which correspond to points of period 19 and 38 for $\mathrm{g} = 9.746$ and $\mathrm{g} = 9.7661$, respectively. As the parameter g increases, there occurs a sequence of period-doubling bifurcations of period 19–38–76–152–304–608, giving rise to a strange Feigenbaum attractor [27], whose portrait is shown in Figs. 6 ($\mathrm{g} = 9.768522$) and 7 ($\mathrm{g} = 9.768526$). As the parameter g increases further to 9.76853, the attractor grows in size and evolves into a chaotic attractor taking up a large area on the map, as shown in Fig. 8.

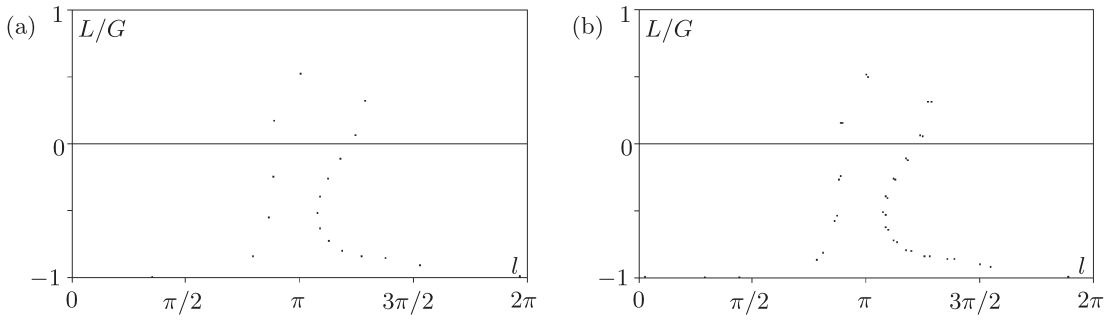

Fig. 5. Poincaré section for regimes with period 19 (a) and 38 (b). The images have been built for the parameters $\mathrm{g} = 9.746$ (a) and $\mathrm{g} = 9.7661$ (b).

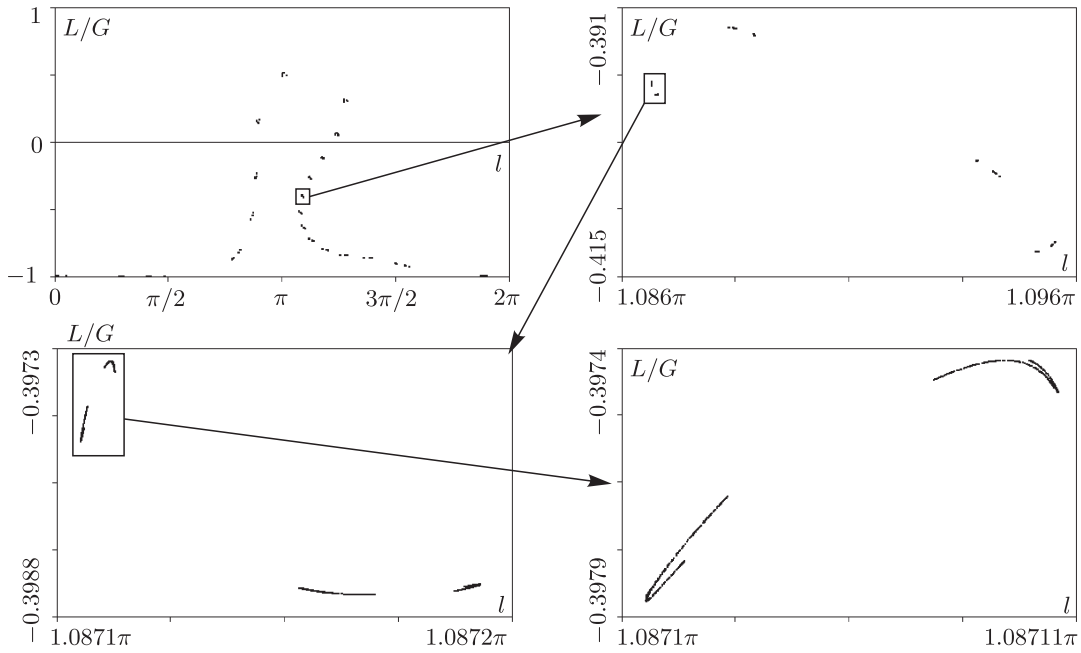

Fig. 6. Poincaré section and its enlarged fragments for g = 9.768522. A sequence of period-doubling bifurcations based on the stable point of period 19 gives rise to a strange Feigenbaum attractor.

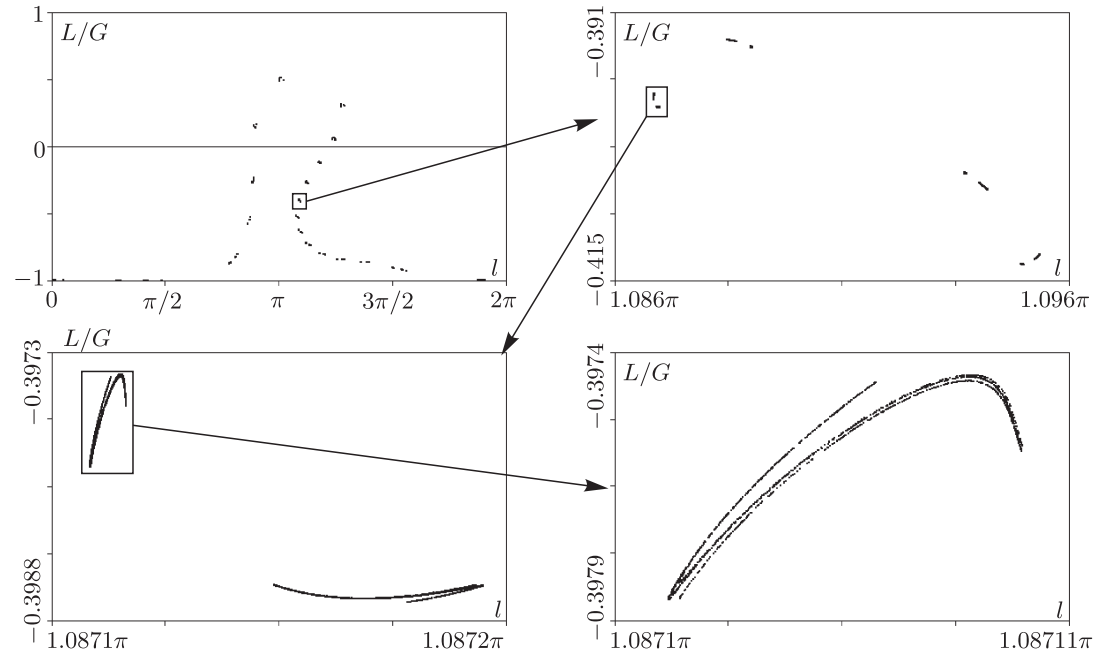

Fig. 7. Poincaré section and its enlarged fragments for g = 9.768526. A sequence of period-doubling bifurcations based on the stable point of period 19 gives rise to a strange Feigenbaum attractor.

The transition to chaos via a sequence of period-doubling bifurcations can also be illustrated by the bifurcation tree shown in Fig. 9.

Estimating the distances between successive period-doubling bifurcations and calculating their relations

$$\delta_F = \frac{\mathrm{g}_n - \mathrm{g}_{n-1}}{\mathrm{g}_{n+1} - \mathrm{g}_n},$$

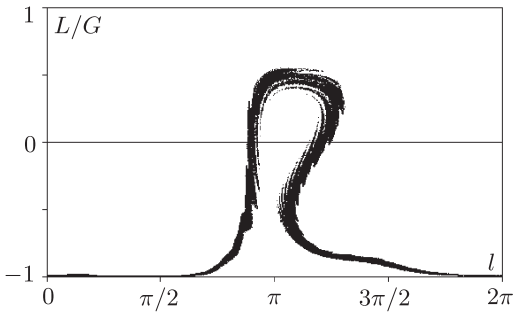

Fig. 8. Poincaré section for g = 9.76853.

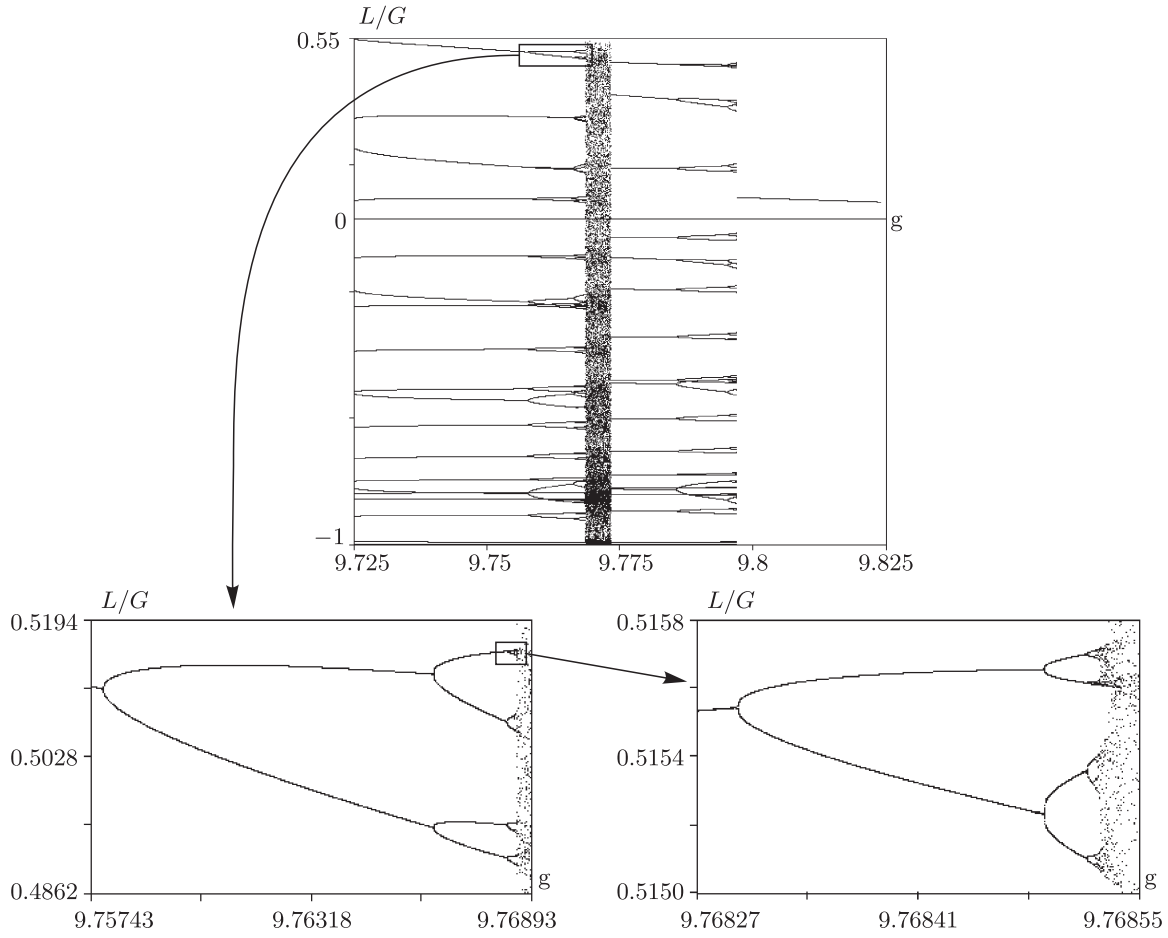

Fig. 9. Tree of period-doubling bifurcations on the plane $(\mathrm{g}, L/G)$.

where g_i is the value of the parameter g at which the ith period-doubling bifurcation occurs, we obtain the following approximations of the Feigenbaum constant:

	$(19,38)/(38,76)$	$(38,76)/(76,152)$
δ_F	3.86	4.45

For dissipative systems, as the transition to chaos occurs according to the Feigenbaum scenario, the above values must tend to the universal constant $\delta_F = 4.6692\ldots$, and this is exactly what we observe already after several period-doubling bifurcations. Further period-doubling bifurcations

occur on very small scales, and so it is not possible to estimate the subsequent approximations of the constant with sufficient accuracy.

4. AVERAGE DIVERGENCE OF THE SYSTEM

A characteristic feature of systems with nonholonomic dissipation is that regions where the phase volume contracts and extends coexist in phase space. In other words, a divergence in such systems is alternating in sign. To illustrate this effect in the system under consideration, we will construct charts of time-average divergence $\langle \int_t \operatorname{div} \boldsymbol{v}(\boldsymbol{x}) dt \rangle$, where $\boldsymbol{v}(\boldsymbol{x})$ is the vector field on the phase space, $\boldsymbol{x} = (\boldsymbol{\omega}, \boldsymbol{\gamma})$. We will calculate the average divergence for the parameters corresponding to the strange chaotic attractor (attractor II) and, for comparison, for parameters under which the system has only simple attractors, and we will depict it on the plane of initial conditions. Calculation of average divergence for analyzing the chaotic behavior of a system was used in [39, 41].

Figure 10 shows charts of the time-average divergence on the plane of initial conditions $(l, L/G)$. It is evident from the figure that the initial distribution of divergence (Fig. 10, $t = 0$) is quite regular, with pronounced regions of positive (shades of yellow and red) and negative (shades of blue) values. Similar diagrams (for $t = 0$) were used in [39] to analyze the dynamics in reversible nonconservative maps.

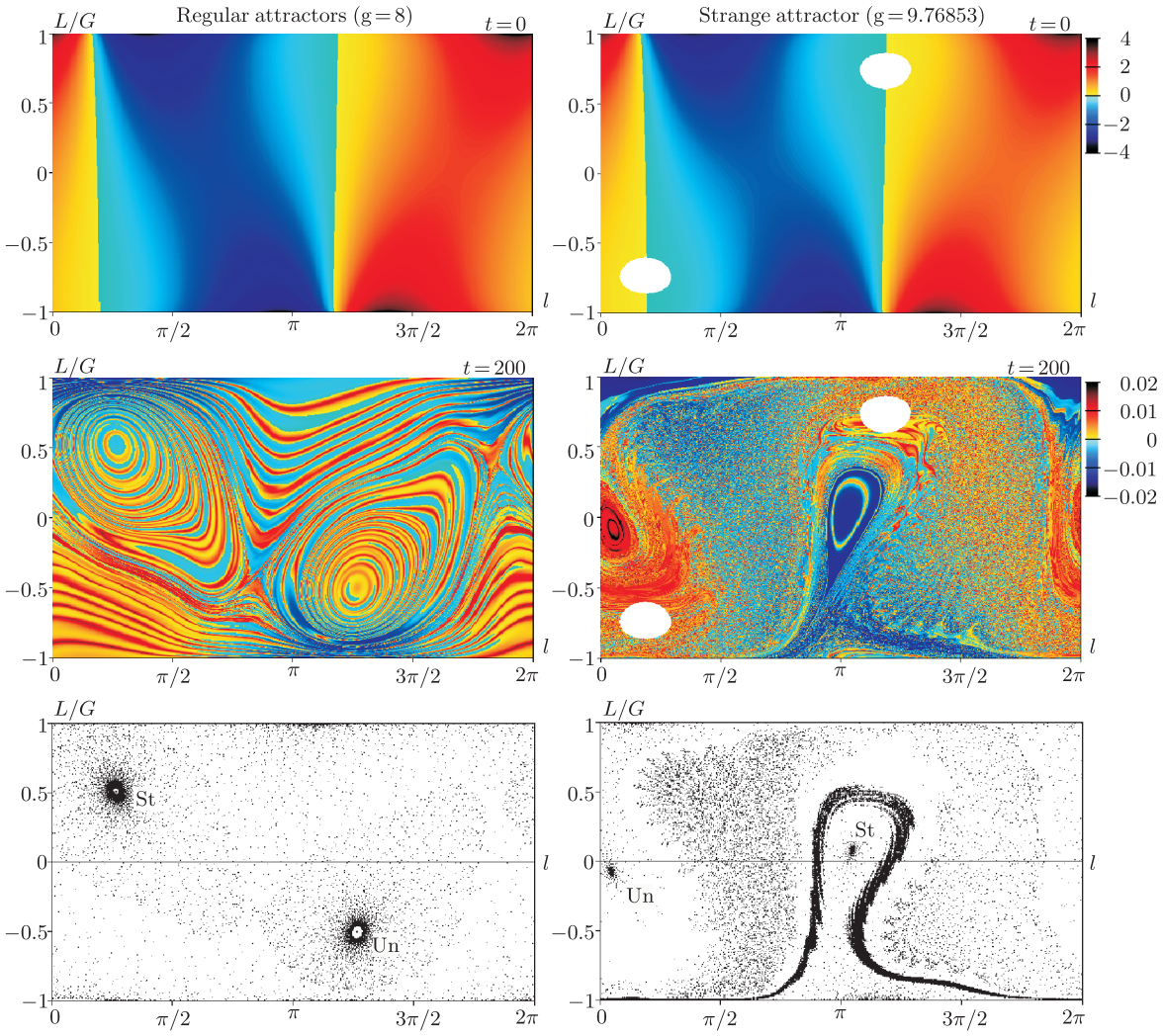

Fig. 10. Chart of time-average divergence on the plane of initial conditions for $t = 0$ (top row), $t = 200$ (middle row), and corresponding sections of the Poincaré map (bottom row) for regular (g = 8, left) and strange (g = 9.76853, right) attractors. The color scheme is shown on the right of the figures. The symbols St and Un on the Pioncaré sections correspond to stable and unstable fixed points, respectively.

Figure 10 shows a transient process of mixing the regions of contraction and extension of phase volume for $t = 200$. As is seen from this figure, regions with positive and negative divergence are strongly mixed in the course of time (Fig. 10, $t = 200$).

Thus, we can conclude that attractor II is, on the one hand, quasi-Hamiltonian (quasi-conservative) since, like a stochastic layer in Hamiltonian mechanics, it takes up a large area in the phase space. On the other hand, inside this attractor there are many stable periodic orbits. In contrast to Hamiltonian mechanics, where the stochastic layer has infinitely many elliptic resonances, the question of finiteness of foci in an attractor has, as far as we know, not yet been completely solved [28]. Thus, the analysis of time-average divergence charts allows us to identify regions of phase space where chaotic attractors can be found.

These figures show once again the specificity of arising attractors, which is related to non-holonomic dissipation [9]. The nature and scenarios of birth of these attractors require additional research.

Remark. Calculation of the average divergence for large times was carried out in [41] to determine parameters under which a contraction of the phase volume occurs. In our system, the phase volume contracts at all parameter values shown in the chart of dynamical regimes (see Fig. 11, shades of blue correspond to negative values of divergence).

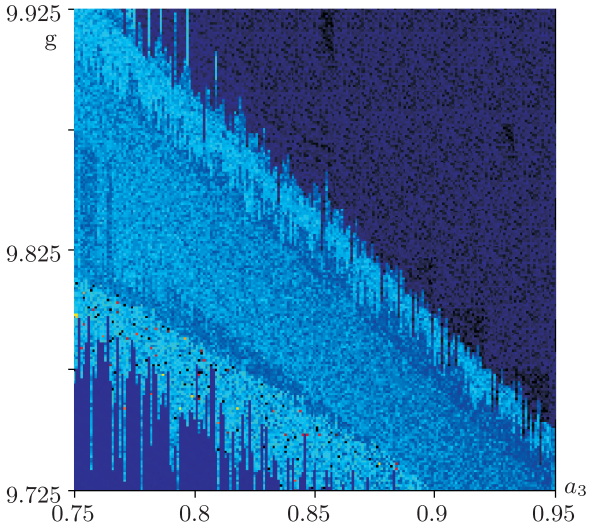

Fig. 11. Chart of average divergence for $t = 2 \cdot 10^4$ on the plane of parameters (a_3, g). Shades of blue correspond to negative values of divergence.

5. ANALYSIS OF THE BEHAVIOR OF THE CONTACT POINT

From the viewpoint of mechanics and modeling of mechanical systems it would be interesting to observe the behavior of the contact point, since the trajectory of the system can be observed and analyzed immediately in experiments. We present the trajectories of the contact point for the attractors obtained above. Note that when constructing the trajectory of the contact point we did not take into account possible losses of contact of the top with the surface, which can occur due to the displacement of the center of mass (as a consequence, with variable reaction of the plane). This issue requires a separate study since paradoxical situations can arise, as described in [29, 30].

The evolution of the contact point of the system is described by the kinematic relations (1.2)

$$\dot{x} = R(\boldsymbol{\beta}, \boldsymbol{\omega}), \qquad \dot{y} = -R(\boldsymbol{\alpha}, \boldsymbol{\omega}).$$

Figures 12–14 show the trajectories of the contact point which correspond to the Poincaré maps presented above. As is evident from these figures, the smaller the area the attractor occupies on the phase plane, the more regular the behavior of the contact point. This conclusion can be

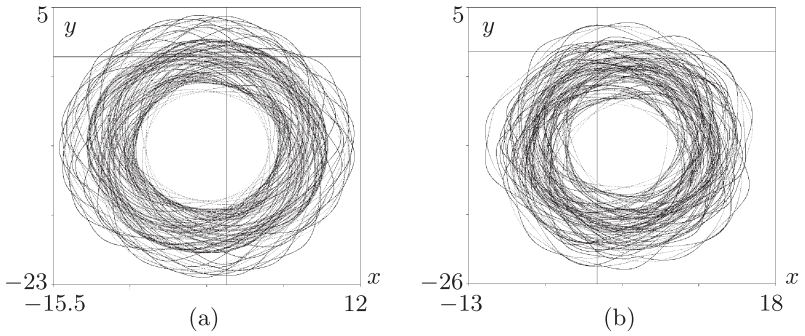

Fig. 12. Trajectories of the point of contact which correspond to periodic regimes 19 (a) and 38 (b) shown in Fig. 5 for 10^3 iterations of the Poincaré map.

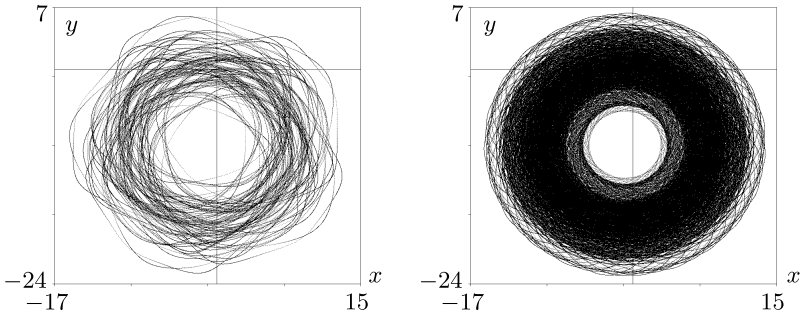

Fig. 13. Trajectory of the point of contact which corresponds to the Feigenbaum attractor shown in Fig. 6 for $g = 9.768522$ for 10^3 (left) and $4 \cdot 10^3$ (right) iterations of the Poincaré map. Due to small differences between the values of the parameter g in Figs. 6 and 7, the trajectories for these two attractors are visually indistinguishable, so we do not present here the trajectory of the contact point that corresponds to Fig. 7.

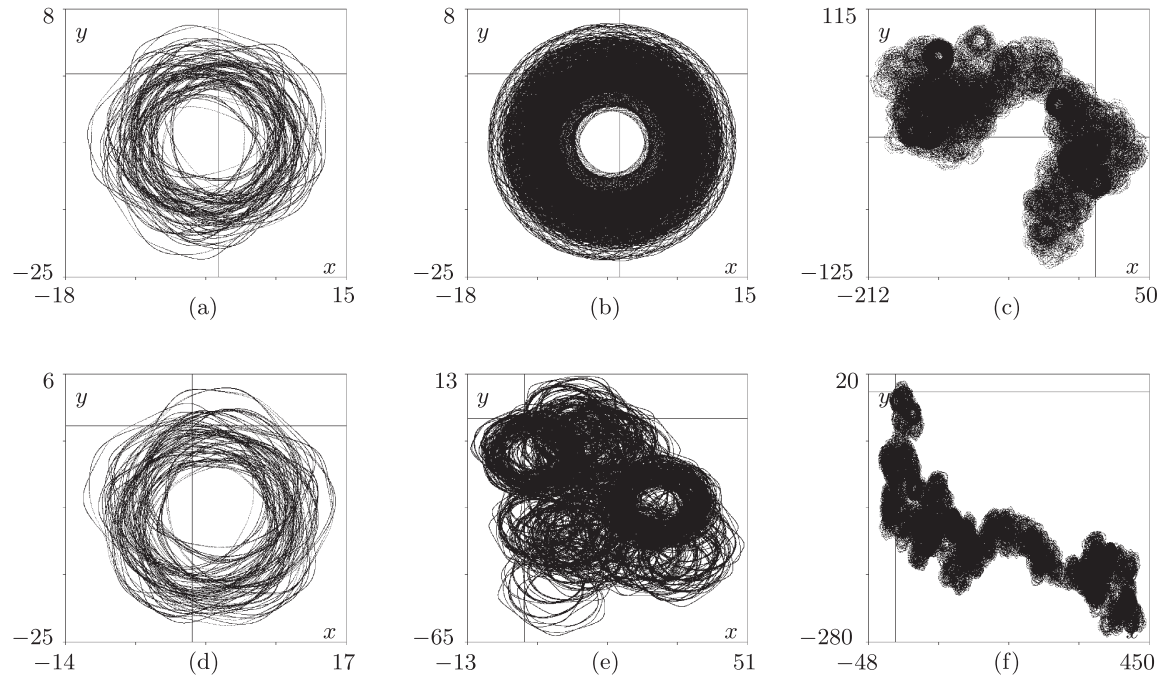

Fig. 14. Trajectories of the point of contact for the attractor shown in Fig. 8 for various (close) initial conditions and for 10^3 (a), (d), $4 \cdot 10^3$ (b), (e) and $2 \cdot 10^5$ (c), (f) iterations of the Poincaré map, respectively, at $g = 9.76853$.

illustrated numerically by calculating the dimension of the attractor, its stochastic characteristic, by the Kaplan – Yorke formula [33]:

$$D = m + \left(\sum_{i=1}^{m} \Lambda_i\right) \Big/ |\Lambda_{m+1}|,$$

where m is the number of Lyapunov exponents, the sum of which is nonnegative.

The system under consideration has two nonzero Lyapunov exponents. The Lyapunov exponents for the attractor shown in Fig. 8 (the corresponding trajectory is depicted in Fig. 14) have the form

$$\Lambda_1 = 0.019069 \pm 0.000479,$$
$$\Lambda_2 = -0.021845 \pm 0.000489,$$
$$\Lambda_1 + \Lambda_2 = -0.002798 \pm 0.000032.$$

Thus, the dimension of the attractor according to Kaplan – Yorke is

$$D = 1 + \frac{\Lambda_1}{|\Lambda_2|} \approx 1.87.$$

For the Feigenbaum attractor shown in Fig. 7 (the trajectory is depicted in Fig. 13) the Lyapunov exponents and the dimension of the attractor are, respectively,

$$\Lambda_1 = 0,000925 \pm 0.000028,$$
$$\Lambda_2 = -0.003315 \pm 0.000036$$
$$\Lambda_1 + \Lambda_2 = -0.002418 \pm 0.000014,$$
$$D \approx 1.28.$$

Thus, the dimension of the Feigenbaum attractor is close to 1. As a consequence, the pattern of the trajectory of the contact point is nearly quasi-periodic.

We also present the Lyapunov exponents and the dimension of attractor I which were calculated in [34]:

$$\Lambda_1 = 0.083368 \pm 0.000422,$$
$$\Lambda_2 = -0.084553 \pm 0.000423$$
$$\Lambda_1 + \Lambda_2 = -0.001184 \pm 0.000011,$$
$$D \approx 1.99.$$

As can be seen, its dimension is close to 2, and this (quasi-)attractor occupies a considerable area in the Poincaré section. A typical trajectory of the contact point for this attractor is shown in Fig. 15.

Thus, for the Feigenbaum attractor (Fig. 7) with dimension $D = 1.28$ the point of contact quasi-periodically sweeps out the area of a ring. For attractor II (Fig. 8) with dimension $D = 1.87$ the trajectory of the contact point exhibits chaotic behavior; however, the Chaplygin top moving on the plane executes many rotations similar to those which are observed on the Feigenbaum attractor. For attractor I (Fig. 3b), for which $D = 1.99$, the motion of the top on the plane is maximally chaotic. This allows the following conclusion: the larger the dimension of the attractor, and hence the larger the area it occupies in the Poincaré section, the more chaotic the behavior of the point of contact.

Following [13, 32], we calculate the quantitative characteristic of the diffusion of the trajectory of the contact point. By diffusion we mean a random (chaotic) pattern of the trajectory of the contact point. Since the trajectories corresponding to stable fixed points are periodic and sweep out the area of a ring on the plane (x, y), we choose the following function to characterize the diffusion:

$$D = \sqrt{(\langle x\rangle - x_n)^2 + (\langle y\rangle - y_n)^2},$$
$$\langle x\rangle = \frac{1}{n}\sum_{i=1}^{n} x_i, \qquad \langle y\rangle = \frac{1}{n}\sum_{i=1}^{n} y_i,$$

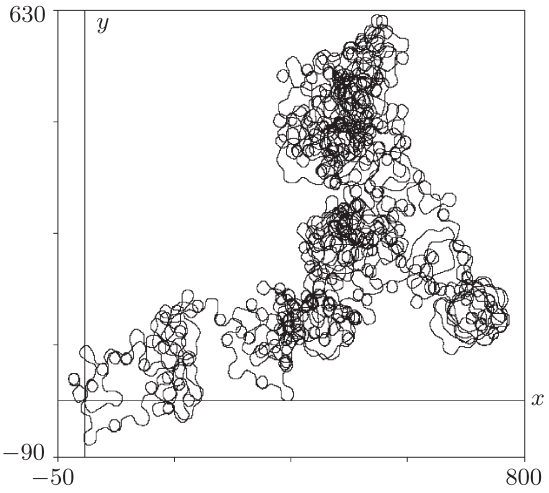

Fig. 15. Trajectory of the contact point which corresponds to the attractor I shown in Fig. 3a.

where (x_n, y_n) is the end point of the trajectory. That is, we shall search for the distance between the averaged value of the trajectory and the end point.

As in the previous section, to demonstrate the behavior of the trajectory of the system during the transition from order to chaos with a constant value of the displacement of the center of mass, $a_3 = 0.9$, we changed the parameter g from 9.725 to 9.825 (i. e., we moved on the chart again from below upwards).

Figure 16 shows a graph of the dependence of the square root of the distance between the averaged value and the end point of the trajectory, $\sqrt{D}$, on the parameter g. The resulting graph can be divided visually into 5 parts, to each of which there corresponds a certain regime of motion (behavior of the point of contact). In region I (in the range of the parameter g from 9.725 to 9.76853) the behavior of the point of contact is regular, and the values of $\sqrt{D}$ lie in the range not exceeding the "width of the ring" whose area is swept out by the trajectory on the plane. Further, in region II (g changes from 9.7685 to 9.7728) the trajectories on the phase plane evolve to attractor II, and the behavior of the point of contact becomes chaotic. Indeed, it can be seen from Fig. 16 that under small changes in the parameter the values of the square root of the distance between the averaged value and the end point of the trajectory are absolutely different. In region III from 9.7728 to 9.7862 the trajectories on the phase plane evolve again to the periodic point, therefore the behavior of the point of contact becomes regular, and, just as in the initial region, the values of $\sqrt{D}$ lie in the range not exceeding the "width of the ring" whose area is swept out by the trajectory on the plane. Of particular interest is region IV (in the range of changing g from 9.7862 to 9.7971). It turns out that in this region the trajectory of the point of contact is regular too, but the (external and internal) radius of the ring swept out by the point of contact increases as the parameter g increases to 9.79416, and then the radius decreases. Finally, in region V all trajectories on the map are attracted to the fixed point of period 1, and hence the point of contact exhibits regular behavior, and the values of $\sqrt{D}$ do almost not change.

As the main result of analysis of the behavior of the contact point we point out the following fact. On each regular attractor, the point of contact of the Chaplygin top exhibits quasi-periodic (that is, regular) behavior. Initially it was assumed that on the strange attractors the point of contact has chaotic behavior. However, the experimental results have shown that chaos on the attractor does not always lead to chaotic behavior of the contact point. In order for the trace of the contact point to exhibit chaotic behavior, it is also necessary that the strange attractor takes up a volume in the phase space that is comparable with the dimension of the phase space itself, otherwise the point of contact will display quasi-periodic behavior.

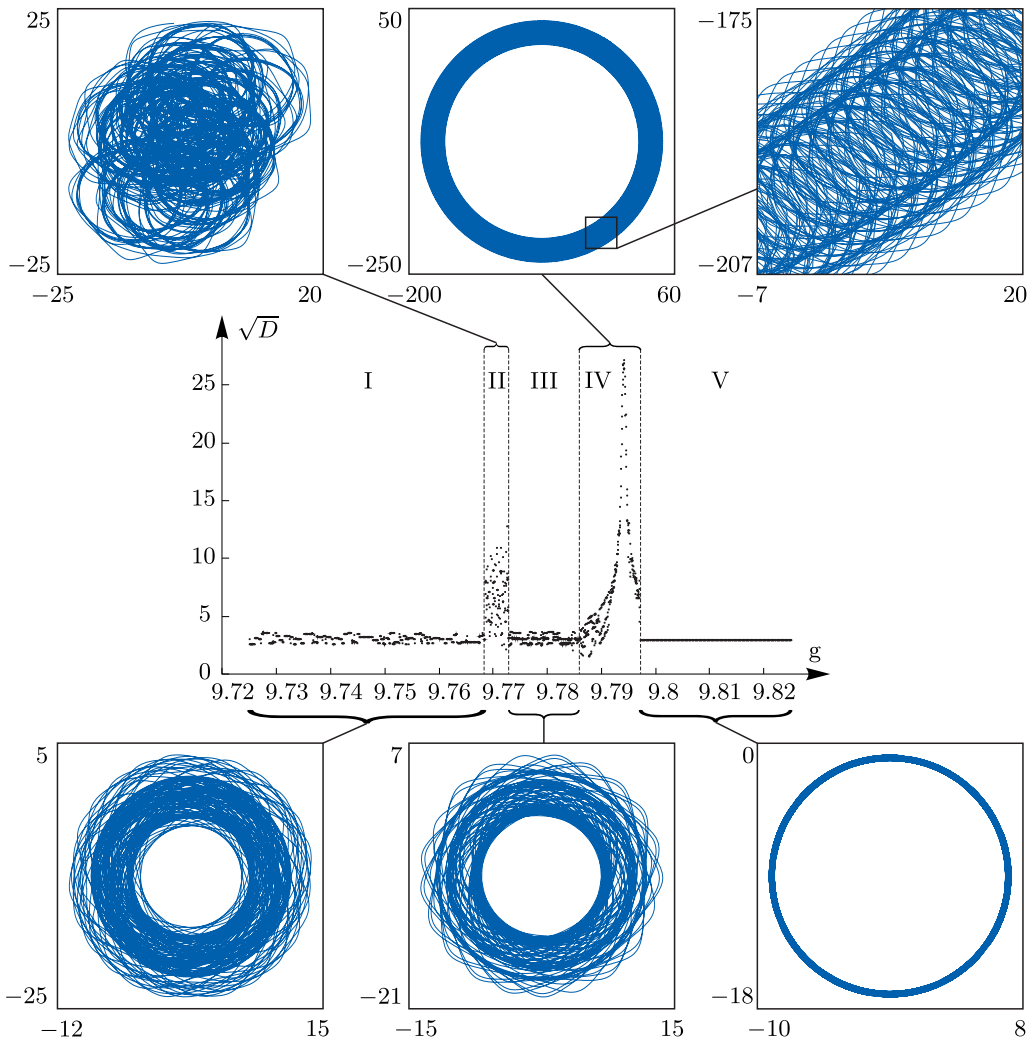

Fig. 16. Square root of the distance between the averaged value and the end point of the trajectory of the Chaplygin top and the characteristic trajectories of the contact point which correspond to each segment.

6. GENEALOGY OF SEPARATRICES BETWEEN ATTRACTORS

Further, we consider scenarios of transition between two attractors described in Section 2.

The transition from the attractor shown in Fig. 3b to the attractor shown in Fig. 3a occurs by rearranging the separatrices of saddle points which bound the domains of attraction of the attractors. Let us observe how the separatrices of hyperbolic points rearrange themselves as the parameter a_3 changes.

The charts of dynamical regimes and numerical analysis of the Poincaré map show that in the area of the attractor at the parameter value $a_3 = 0.9$ there coexist many different points of different periods, which arise via saddle-node bifurcations. Moreover, a dense set of separatrices of saddle points is formed. As is seen from Fig. 17, the domain of attraction of attractor II ($a_3 = 0.9$) is bounded by stable (blue) separatrices of saddle points P, Q, R (shown as green points in the figure). As the parameter a_3 decreases, the domain of attraction of attractor II shrinks, while the set of separatrices of saddle points inside the attractor increases. This results in a destruction of attractor II, and the trajectories begin to sweep out most of the phase plane. As the parameter a_3 decreases further to the value 0.5, the separatrices of the saddle points P, Q, R, S rearrange themselves in such a way that almost all trajectories evolve to the domain of attraction of attractor I. In [34] it is shown that, when $a_3 = 0.5$, this domain becomes invariant, that is, when the trajectories enter this domain, they do not leave it. A detailed description of the scenario of birth of attractor I is given in [34, 35].

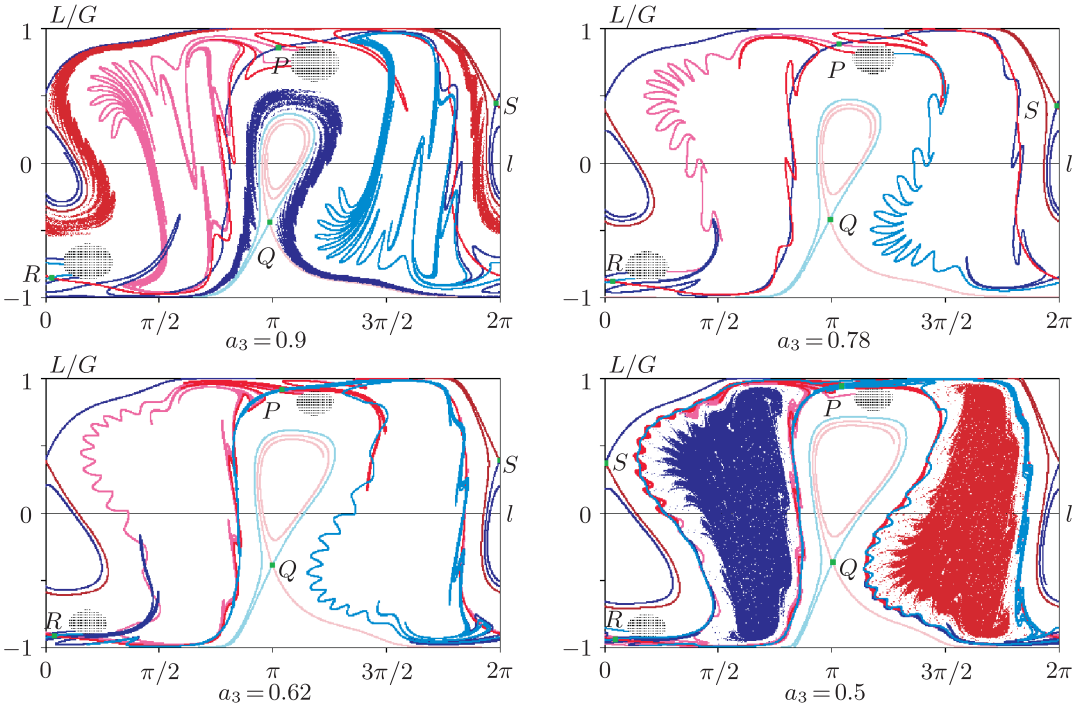

Fig. 17. Rearrangement of the separatrices of saddle points P, Q, R, S under the change of the projection of the vector of displacement of the center of mass a_3 from 0.9 to 0.5. Shades of blue denote stable separatrices of hyperbolic points, shades of red correspond to unstable ones. The hatched areas correspond to regions of prohibited motion.

CONCLUSION

This paper presents a systematic analysis of regular and chaotic behavior of the rubber model of the Chaplygin top. In this system, a Feigenbaum attractor is found and explored and the scenario of its birth is described. A preliminary analysis of the behavior of the contact point depending on the characteristics of the corresponding attractor is carried out.

It turns out that the dynamics of the contact point in the system is regular due to multistability and due to the fact that the phase space contains, as a rule, only simple attractors. For this reason, the search for strange chaotic attractors, on which the behavior of the system also becomes chaotic, is of particular interest for physical applications. As mentioned previously, this can be used especially in chaos control and stabilization theory, which is being developed nowadays. It would also be interesting to experimentally discover effects which are observed in the system under study (for example, the changes of regular and chaotic regimes under small changes in the system parameters). Similar behavior of the contact point for the marble model is discussed in [9], where the Poincaré map of the system is three-dimensional and the dynamics is much more diverse.

Another possible avenue of further research aimed at developing the results of this paper is to study a related problem, that of a Chaplygin top rolling on a sphere using the rubber model. In spite of the existence of an invariant measure, this system is chaotic even when there is no displacement of the center of mass [26]. One interesting integrable case of this problem was found and studied in [17] (its marble analog was found much earlier [5, 6, 18]). This case takes place when there is a certain ratio between the radius of a fixed sphere and that of a moving sphere.

ACKNOWLEDGMENTS

The authors express their gratitude to S. P. Kuznetsov, I. S. Mamaev, I. R. Sataev and A. A. Kilin for fruitful discussions and useful comments.

The work of A. V. Borisov (Introduction, Sections 1, 4 and 6) was carried out within the framework of the Grant of the Russian Science Foundation No. 15-12-20035. The work of A. O. Kazakov (Sections 2 and 3) was supported by the Basic Research Program at the National Research University Higher School of Economics (project 98) and by the RFBR grants No. 16-01-00364

and No. 14-01-00344. The work of E. N. Pivovarova (Section 5 and Conclusion) was supported by the Russian Foundation for Basic Research (project No. 15-08-09261-a).

The computer simulation was carried out using the software package "Computer Dynamics: Chaos" (http://lab-en.ics.org.ru/lab/page/kompyuternaya-dinamika/).

REFERENCES

1. Afraimovich, V. S. and Shil'nikov, L. P., Strange Attractors and Quasiattractors, in *Nonlinear Dynamics and Turbulence,* G. I. Barenblatt, G. Iooss, D. D. Joseph (Eds.), Interaction Mech. Math. Ser., Boston, Mass.: Pitman, 1983, pp. 1–34.
2. Armour, R. H. and Vincent, J. F. V., Rolling in Nature and Robotics: A Review, *J. Bionic Eng.,* 2006, vol. 3, no. 4, pp. 195–208.
3. Bizyaev, I. A., Nonintegrability and Obstructions to the Hamiltonianization of a Nonholonomic Chaplygin Top, *Dokl. Math.,* 2014, vol. 90, no. 2, pp. 631–634; see also: *Dokl. Akad. Nauk,* 2014, vol. 458, no. 4, pp. 398–401.
4. Bolsinov, A. V., Borisov, A. V., and Mamaev, I. S., Rolling of a Ball without Spinning on a Plane: The Absence of an Invariant Measure in a System with a Complete Set of Integrals, *Regul. Chaotic Dyn.,* 2012, vol. 17, no. 6, pp. 571–579.
5. Borisov, A. V. and Fedorov, Yu. N., On Two Modified Integrable Problems in Dynamics, *Mosc. Univ. Mech. Bull.,* 1995, vol. 50, no. 6, pp. 16–18; see also: *Vestnik Moskov. Univ. Ser. 1. Mat. Mekh.,* 1995, no. 6, pp. 102–105.
6. Borisov, A. V., Fedorov, Yu. N., and Mamaev, I. S., Chaplygin Ball over a Fixed Sphere: An Explicit Integration, *Regul. Chaotic Dyn.,* 2008, vol. 13, no. 6, pp. 557–571.
7. Borisov, A. V., Jalnine, A. Yu., Kuznetsov, S. P., Sataev, I. R., and Sedova, J. V., Dynamical Phenomena Occurring due to Phase Volume Compression in Nonholonomic Model of the Rattleback, *Regul. Chaotic Dyn.,* 2012, vol. 17, no. 6, pp. 512–532.
8. Borisov, A. V., Kazakov, A. O., and Sataev, I. R., The Reversal and Chaotic Attractor in the Nonholonomic Model of Chaplygin's Top, *Regul. Chaotic Dyn.,* 2014, vol. 19, no. 6, pp. 718–733.
9. Borisov, A. V., Kazakov, A. O., and Sataev, I. R., Spiral Chaos in the Nonholonomic Model of a Chaplygin Top, *Regul. Chaotic Dyn.,* 2016, vol. 21, nos. 7–8, pp. 939–954.
10. Borisov, A. V., Kilin, A. A., and Mamaev, I. S., How to Control Chaplygin's Sphere Using Rotors, *Regul. Chaotic Dyn.,* 2012, vol. 17, nos. 3–4, pp. 258–272.
11. Borisov, A. V., Kilin, A. A., and Mamaev, I. S., How to Control Chaplygin's Sphere Using Rotors: 2, *Regul. Chaotic Dyn.,* 2013, vol. 18, nos. 1–2, pp. 144–158.
12. Borisov, A. V., Kilin, A. A., and Mamaev, I. S., The Problem of Drift and Recurrence for the Rolling Chaplygin Ball, *Regul. Chaotic Dyn.,* 2013, vol. 18, no. 6, pp. 832–859.
13. Borisov, A. V. and Kuznetsov, S. P., Regular and Chaotic Motions of a Chaplygin Sleigh under Periodic Pulsed Torque Impacts, *Regul. Chaotic Dyn.,* 2016, vol. 21, nos. 7–8, pp. 792–803.
14. Borisov, A. V. and Mamaev, I. S., Strange Attractors in Rattleback Dynamics, *Physics–Uspekhi,* 2003, vol. 46, no. 4, pp. 393–403; see also: *Uspekhi Fiz. Nauk,* 2003, vol. 173, no. 4, pp. 407–418.
15. Borisov, A. V. and Mamaev, I. S., *Rigid Body Dynamics: Hamiltonian Methods, Integrability, Chaos,* Izhevsk: R&C Dynamics, Institute of Computer Science, 2005 (Russian).
16. Borisov, A. V. and Mamaev, I. S., Isomorphism and Hamilton Representation of Some Nonholonomic Systems, *Siberian Math. J.,* 2007, vol. 48, no. 1, pp. 26–36; see also: *Sibirsk. Mat. Zh.,* 2007, vol. 48, no. 1, pp. 33–45.
17. Borisov, A. V. and Mamaev, I. S., Conservation Laws, Hierarchy of Dynamics and Explicit Integration of Nonholonomic Systems, *Regul. Chaotic Dyn.,* 2008, vol. 13, no. 5, pp. 443–490.
18. Borisov, A. V. and Mamaev, I. S., Topological Analysis of an Integrable System Related to the Rolling of a Ball on a Sphere, *Regul. Chaotic Dyn.,* 2013, vol. 18, no. 4, pp. 356–371.
19. Borisov, A. V. and Mamaev, I. S., The Rolling Motion of a Rigid Body on a Plane and a Sphere: Hierarchy of Dynamics, *Regul. Chaotic Dyn.,* 2002, vol. 7, no. 2, pp. 177–200.
20. Borisov, A. V., Mamaev, I. S., and Bizyaev, I. A., The Hierarchy of Dynamics of a Rigid Body Rolling without Slipping and Spinning on a Plane and a Sphere, *Regul. Chaotic Dyn.,* 2013, vol. 18, no. 3, pp. 277–328.
21. Borisov, A. V., Mamaev, I. S., and Bizyaev, I. A., Historical and Critical Review of the Development of Nonholonomic Mechanics: The Classical Period, *Regul. Chaotic Dyn.,* 2016, vol. 21, no. 4, pp. 455–476.
22. Borisov, A. V., Mamaev, I. S., and Kilin, A. A., Rolling of a Ball on a Surface: New Integrals and Hierarchy of Dynamics, *Regul. Chaotic Dyn.,* 2002, vol. 7, no. 2, pp. 201–220.
23. Chaplygin, S. A., On a Ball's Rolling on a Horizontal Plane, *Regul. Chaotic Dyn.,* 2002, vol. 7, no. 2, pp. 131–148; see also: *Math. Sb.,* 1903, vol. 24, no. 1, pp. 139–168.
24. Chase, R. and Pandya, A., A Review of Active Mechanical Driving Principles of Spherical Robots, *Robotics,* 2012, vol. 1, no. 1, pp. 3–23.

25. Crossley, V. A., *A Literature Review on the Design of Spherical Rolling Robots,* Pittsburgh, Pa., 2006. 6 pp.
26. Ehlers, K. M. and Koiller, J., Rubber Rolling: Geometry and Dynamics of $2-3-5$ Distributions, in *Proc. IUTAM Symposium 2006 on Hamiltonian Dynamics, Vortex Structures, Turbulence (Moscow, Russia, 25–30 August 2006),* pp. 469–480.
27. Feigenbaum, M. J., Universal Behavior in Nonlinear Systems, *Phys. D,* 1983, vol. 7, nos. 1–3, pp. 16–39.
28. Feudel, U., Grebogi, C., Hunt, B. R., and Yorke, J. A., Map with More Than 100 Coexisting Low-Period Periodic Attractors, *Phys. Rev. E*, 1996, vol. 54, no. 1, pp. 71–81.
29. Ivanov, A. P., On Detachment Conditions in the Problem on the Motion of a Rigid Body on a Rough Plane, *Regul. Chaotic Dyn.*, 2008, vol. 13, no. 4, pp. 355–368.
30. Ivanov, A. P., Geometric Representation of Detachment Conditions in Systems with Unilateral Constraint, *Regul. Chaotic Dyn.*, 2008, vol. 13, no. 5, pp. 435–442.
31. Ivanov, A. P., On Final Motions Of a Chaplygin Ball on a Rough Plane, *Regul. Chaotic Dyn.,* 2016, vol. 21, nos. 7–8, pp. 804–810.
32. Jung, P., Marchegiani, G., and Marchesoni, F., Nonholonomic Diffusion of a Stochastic Sled, *Phys. Rev. E,* 2016, vol. 93, no. 1, 012606, 9 pp.
33. Kaplan, J. L. and Yorke, J. A., A Chaotic Behavior of Multi-Dimensional Differential Equations, in *Functional Differential Equations and Approximations of Fixed Points,* H.-O. Peitgen and H.-O. Walther (Eds.), Lecture Notes in Math., vol. 730, Berlin: Springer, 1979, pp. 204–227.
34. Kazakov, A. O., Strange Attractors and Mixed Dynamics in the Problem of an Unbalanced Rubber Ball Rolling on a Plane, *Regul. Chaotic Dyn.,* 2013, vol. 18, no. 5, pp. 508–520.
35. Kazakov, A. O., On the Chaotic Dynamics of a Rubber Ball with Three Internal Rotors, *Nonlinear Dynamics & Mobile Robotics,* 2014, vol. 2, no. 1, pp. 73–97.
36. Kilin, A. A., The Dynamics of Chaplygin Ball: The Qualitative and Computer Analysis, *Regul. Chaotic Dyn.,* 2001, vol. 6, no. 3, pp. 291–306.
37. Marsden, J. E. and Ross, Sh. D., New Methods in Celestial Mechanics and Mission Design, *Bull. Amer. Math. Soc. (N. S.),* 2006, vol. 43, no. 1, pp. 43–73.
38. Ott, E., Grebogi, C., and Yorke, J. A., Controlling Chaos, *Phys. Rev. Lett.,* 1990, vol. 64, no. 11, pp. 1196–1199.
39. Roberts, J. A. G. and Quispel, G. R. W., Chaos and Time-Reversal Symmetry. Order and Chaos in Reversible Dynamical Systems, *Phys. Rep.*, 1992, vol. 216, nos. 2–3, pp. 63–177.
40. Sataev, I. R. and Kazakov, A. O., Scenarios of Transition to Chaos in the Nonholonomic Model of a Chaplygin Top, *Nelin. Dinam.,* 2016, vol. 12, no. 2, pp. 235–250 (Russian).
41. Topaj, D. and Pikovsky, A., Reversibility vs. Synchronization in Oscillator Lattices, *Phys. D*, 2002, vol. 170, no. 2, pp. 118–130.